



### Voltage-activated elementary calcium release events in isolated mouse skeletal muscle fibers

Journal:	<i>Journal of Membrane Biology</i>
Manuscript ID:	JMB-H-08-0029.R2
Manuscript Type:	Articles
Date Submitted by the Author:	n/a
Complete List of Authors:	Csernoch, Laszlo; University of Debrecen, Physiology Pouvreau, Sandrine; University Lyon 1, Physiology-UMR 5123 Ronjat, Michel; University Joseph Fourier, Institut des Neurosciences-Inserm U386 Jacquemond, Vincent; University Lyon 1, Physiology-UMR 5123
Keywords:	calcium regulation and EC coupling in muscle, ion channels in sarcoplasmic reticulum of striated muscle, Mechanisms of calcium influx, Modulation of excitation-contraction coupling, ryanodine receptors, ryanodine receptor studies, Voltage Clamp Studies



1  
2  
3  
4  
5  
6  
7  
8  
9  
10  
11  
12  
13  
14  
15  
16  
17  
18  
19  
20  
21  
22  
23  
24  
25  
26  
27  
28  
29  
30  
31  
32  
33  
34  
35  
36  
37  
38  
39  
40  
41  
42  
43  
44  
45  
46  
47  
48  
49  
50  
51  
52  
53  
54  
55  
56  
57  
58  
59  
60

# Voltage-activated elementary calcium release events in isolated mouse skeletal muscle fibers

Laszlo Csernoch<sup>\*</sup>, Sandrine Pouvreau<sup>†</sup>, Michel Ronjat<sup>‡</sup> and Vincent Jacquemond<sup>†¶</sup>

<sup>†</sup> Physiologie Intégrative Cellulaire et Moléculaire, Université Lyon 1, UMR CNRS 5123, 43 Boulevard du 11 novembre 1918, 69622 Villeurbanne, France.

<sup>\*</sup> Department of Physiology, Medical and Health Science Center, University of Debrecen, P.O. Box 22, Debrecen H-4012, Hungary.

<sup>‡</sup> Grenoble Institut des Neurosciences, Centre de Recherche Inserm U.836, Université Joseph Fourier, BP 170, 38042 Grenoble Cedex 9, France.

<sup>¶</sup> to whom correspondence should be addressed.

Address:

Physiologie Intégrative Cellulaire et Moléculaire

Université Claude Bernard - Lyon 1, UMR CNRS 5123

Bât. Raphael Dubois, 43 boulevard du 11 novembre 1918

F 69622 Villeurbanne Cedex - France

Tel.: (33) 4 72-44-81-64; Fax: (33) 4 72-44-79-37

e-mail: vincent.jacquemond@univ-lyon1.fr

**ABSTRACT**

The elementary  $\text{Ca}^{2+}$  release events underlying voltage activated myoplasmic  $\text{Ca}^{2+}$  transients in mammalian muscle still remain elusive. Here we looked for such events in confocal line-scan  $(x,t)$  images of fluo-3 fluorescence taken from isolated adult mouse skeletal muscle fibers held under voltage-clamp conditions. In response to step depolarizations spatially segregated fluorescence signals could be detected that were riding on a global increase in fluorescence. These discrete signals were separated using digital filtering in the spatial domain; mean values for their spatial half-width and amplitude were  $1.99 \pm 0.09 \mu\text{m}$  and  $0.16 \pm 0.005 \Delta F/F_0$  ( $n=151$ ), respectively. Under control conditions, the duration of the events was limited by the pulse duration, In contrast, in the presence of maurocalcine, a scorpion toxin suspected to disrupt the process of repolarization-induced ryanodine receptor closure, events uninterrupted by the end of the pulse were readily detected. Overall results establish these voltage-activated low amplitude local  $\text{Ca}^{2+}$  signals as inherent components of the physiological  $\text{Ca}^{2+}$  release process of mammalian muscle and suggest that they result from the opening of either one ryanodine receptor or of a coherently operating group of RyRs, under the control of the plasma membrane polarization.

**Keywords:** Excitation-contraction coupling, mammalian skeletal muscle, voltage-clamp, intracellular  $\text{Ca}^{2+}$ , confocal imaging. dihydropyridine receptor, ryanodine receptor.

## INTRODUCTION

In skeletal muscle, contractile activation is triggered by an increase in myoplasmic  $\text{Ca}^{2+}$  concentration due to a  $\text{Ca}^{2+}$  flux from the sarcoplasmic reticulum (SR), through the ryanodine receptor  $\text{Ca}^{2+}$  release channels. This flux is activated upon depolarization of the plasma membrane through interactions between the voltage-sensing dihydropyridine receptors (DHPRs) and the ryanodine receptors (RyRs). Within the past decade the advent of confocal imaging technology has allowed the detection of the elementary activity of intracellular  $\text{Ca}^{2+}$  release channels in living cells, which revolutionized our perception and understanding of the physiological properties and function of these proteins (see for instance Berridge, 2006). Indeed, the possibility to detect such elementary signals is of highest interest because it provides a unique access to the unitary properties of the channels in their native environment. In this regard, the elementary voltage-activated  $\text{Ca}^{2+}$  release events from the SR of skeletal muscle were rapidly identified in isolated frog muscle fibers using a combination of intracellular  $[\text{Ca}^{2+}]$  detection under confocal microscopy together with voltage-clamp (Tsugorka et al., 1995; Klein et al., 1996). In this preparation the global myoplasmic  $\text{Ca}^{2+}$  transient builds up as an accumulation of stereotyped discrete  $\text{Ca}^{2+}$  release events, the  $\text{Ca}^{2+}$  sparks, which, since then, have been extensively characterized (see for recent reviews Baylor, 2005; Klein and Schneider, 2006; Csernoch, 2007). Unexpectedly the situation in mammalian muscle came out to be somewhat more complicated and confusing: in rat fibers, voltage-activated elementary  $\text{Ca}^{2+}$  release events were first thought to be unresolvable (Shirokova et al., 1998) and then a class of local fluorescence signals yielding very different properties from the amphibian  $\text{Ca}^{2+}$  sparks were suggested to correspond to the unitary events in this preparation (Csernoch et al., 2004). The difference between the frog and the rat may be due to a different composition in RyR isoforms (see for instance Pouvreau et al., 2007) but also to

1  
2  
3  
4  
5  
6  
7  
8  
9  
10  
11  
12  
13  
14  
15  
16  
17  
18  
19  
20  
21  
22  
23  
24  
25  
26  
27  
28  
29  
30  
31  
32  
33  
34  
35  
36  
37  
38  
39  
40  
41  
42  
43  
44  
45  
46  
47  
48  
49  
50  
51  
52  
53  
54  
55  
56  
57  
58  
59  
60

other still misunderstood discrepancies in the mechanisms that control the gating of the RyRs in the two preparations. Further investigation of the properties of the elementary calcium release events in mammalian muscle is certainly a key to the comprehension of these differences but also to a full understanding of skeletal muscle function under normal and pathological conditions. The present study aimed at characterizing the properties of the elementary  $\text{Ca}^{2+}$  release events in intact mouse skeletal muscle fibers. We show that, in this preparation, signals having the properties of the previously described “embers” (Gonzalez et al., 2000; Zhou et al., 2003) are activated by membrane depolarization and interrupted by membrane repolarization. A characterization of the properties of these events should be inherent to future studies concerning the *in vivo* function and regulation of the RyR in mammalian muscle. A part of this work has been presented to the Biophysical Society (Csernoch et al., 2006).

## MATERIALS AND METHODS

### *Isolation of the muscle fibers*

Most of the experiments were performed on single skeletal fibers isolated from the *flexor digitorum brevis* muscles of wild-type (Swiss-OF1) male mice. A specific subset of measurements was achieved on fibers isolated from frog toe muscles. All experiments were performed in accordance with the guidelines of the French Ministry of Agriculture (87/848) and of the European Community (86/609/EEC). In brief, mice were killed by cervical dislocation after halothane anesthesia. The muscles were removed and treated with collagenase (Sigma type 1, Sigma-Aldrich, Saint Quentin Fallavier, France) for 60–75 min at 37°C in the presence of Tyrode as external solution. Single fibers were then obtained by triturating the muscles within the experimental chamber. Frog toe muscles were dissected and treated with collagenase using identical procedures.

### *Preparation of skinned muscle fibers*

Single fibers, isolated as detailed above, were mounted into a petri-dish with a glass cover-slip bottom. Fibers were bathed in the presence of a relaxing solution (see Solutions) containing 0.002% saponin for 2–3 min. Permeabilization of the surface membrane was monitored by imaging the fluorescence of fluo-3 present at a concentration of 50  $\mu\text{M}$  into the solution. This solution was then replaced by a  $\text{K}_2\text{SO}_4$ -based internal solution containing 100  $\mu\text{M}$  fluo-3 (see Solutions).

### *Preparation of intact muscle fibers*

Details of procedures for partial insulation of isolated fibers with silicone grease were as described previously (Jacquemond, 1997; Collet et al., 1999). In brief, the major part of a single fiber was electrically insulated with silicone grease so that whole-cell voltage clamp could be achieved on a short portion (50- to 100  $\mu\text{m}$  long) of the fiber extremity. A solution containing 1 mM fluo-3 diluted in an intracellular-like solution was then pressure microinjected into the silicone insulated portion of the fiber. A minimum delay of 20 min was then allowed before voltage-clamping the fibers. Under these conditions the dye was assumed to reach a final concentration within the 100  $\mu\text{M}$  range following intracellular equilibration. In some experiments the injected solution also contained maurocalcine at a concentration of 0.5 mM. All experiments were performed at room temperature (20–22°C), in the presence of a tetraethylammonium (TEA)-containing solution as extracellular medium (see Solutions). [The sarcomere length of the fibers was typically 1.9  \$\mu\text{m}\$ .](#)

### *Electrophysiology*

An RK-400 patch-clamp amplifier (Bio-Logic, Claix, France) was used in whole-cell configuration. Command voltage pulse generation was done with an SMP 300 programmable stimulator (Bio-Logic). Voltage-clamp was performed with a microelectrode filled with the internal-like solution (see Solutions). Analog compensation was systematically used to decrease the effective series resistance. Microelectrode resistance was within 1–3 M $\Omega$ . The tip of the microelectrode was inserted through the silicone, within the insulated part of the fiber. Membrane depolarizations were applied from a holding command potential of -80 mV to values typically ranging between -60 and -40 mV ([with  \$\Delta V\$  increments of 5 mV](#)).

### *Confocal detection of fluo-3 fluorescence and image analysis*

Unless otherwise specified, imaging was achieved on the Zeiss LSM 510 laser scanning confocal microscope available at the *Centre Technologique des Microstructures* of University Lyon 1. The microscope was equipped with a 63x oil immersion objective (NA=1.4). Fluo-3 was excited with the 488-nm line of an argon ion laser and the emitted fluorescent light was measured at wavelengths  $>505$  nm. The point spread function was determined with 100 nm wide fluorescent beads, which gave a full width at half amplitude (FWHM) of 0.3  $\mu\text{m}$  in the  $x$  and  $y$  direction and of 0.8  $\mu\text{m}$  in the  $z$  direction. Line-scan images (512/1024 pixels) were taken with a time resolution of 1.54 ms/line, corresponding to 73.1  $\mu\text{m}$  and 1.58 s. These  $(x,t)$  images were normalized to baseline fluorescence ( $F_0 [x]$ ). The line was always oriented along the longitudinal axis of the fibers. Images taken under voltage-clamp conditions that yielded contractile artifacts were discarded from the analysis.

Elementary  $\text{Ca}^{2+}$  release events in line-scan images taken from skinned fibers were captured using an automatic computer detection method based on previously published algorithms (Cheng et al., 1999), as described earlier (Szentesi et al., 2004). In brief, the program identified elementary events as regions with fluorescence above a relative threshold, calculated from the noise in the image and having amplitude  $> 0.3 \Delta F/F_0$  units. The program also determined the parameters of the identified events: amplitude, spatial half-width measured at the time of the peak (full width at half-maximum, FWHM) and duration. FWHM was obtained from fitting a Gaussian function to the spatial distribution obtained by averaging three lines at the peak of the events.

1  
2  
3 The line-scan images taken from mouse intact fibers stimulated by voltage-clamp  
4 depolarizations were normalized to the baseline fluorescence measured before the pulse. In  
5 practice, 10-30 line-scan images were usually taken in a given fiber. In order to remove the  
6 background fluorescence during the depolarizing pulse (see Results) the images were high-  
7 pass filtered in the space domain using the built-in fast Fourier-transform (FFT) function of  
8 Microcal Origin (Microcal Software Inc., Northampton, MA) software: the steady level and  
9 three lowest frequency components were removed and an inverse Fourier transform was used  
10 to obtain an image devoid of the background increase in fluorescence (this approach assumes  
11 that the background increase is present everywhere and thus is represented with low  
12 frequencies while an event is restricted in space and thus is represented by high frequencies).  
13 Filtered images were then subjected to an event-detecting routine also based on the Cheng et  
14 al. (1999) algorithms. For each event the following parameters were determined: amplitude,  
15 latency, FWHM. For this, three adjacent lines in the space domain, centered at the peak of the  
16 event, were averaged and smoothed 10 times. The x positions of the first and of the last  
17 maximum, within the time course of the event, were then determined by eye. The amplitude  
18 of the event was then calculated as the average value of all points sitting between the first  
19 point in the event that reached 90 % of the first peak and the last point in the event that  
20 reached 90 % of the last peak. Only events with amplitude of  $\Delta F/F_0 \geq 0.1$  were then kept for  
21 the analysis. The latency was determined at the first point along the time course that had a  
22 value equal to 10 % the average amplitude. The duration of the event was taken as the time  
23 between the latency and the last point in the event that reached 90 % of the last peak. The  
24 FWHM was obtained from a Gaussian fit to the average of all lines in the space domain over  
25 the same time interval used for calculation of the amplitude.  
26  
27 The line-scan images taken from frog intact fibers stimulated by voltage-clamp  
28 depolarizations were normalized to the baseline fluorescence measured before the pulse.  
29  
30

1  
2  
3 Sparks were identified using the same event detecting routine as the one used in mouse intact  
4 fibers. The amplitude, latency and FWHM of the voltage-activated  $\text{Ca}^{2+}$  sparks were also  
5 measured using similar procedures and criteria as for the images from the mouse intact fibers.  
6  
7 Only, the amplitude of a spark was calculated as the average value of points sitting between  
8 the first and the last that reached 90 % of the spark central peak amplitude. When the FFT  
9 filter procedure was applied on a spark-containing line-scan image from a frog fiber, the  
10 amplitude and spatial spread of the sparks were slightly reduced whereas their time course  
11 remained unaffected (not illustrated).  
12  
13  
14  
15  
16  
17  
18  
19  
20  
21  
22  
23

### *Solutions*

24 Tyrode solution contained (in mM): 140 NaCl, 5 KCl, 2.5  $\text{CaCl}_2$ , 2  $\text{MgCl}_2$ , and 10 HEPES  
25 adjusted to pH 7.20 with NaOH. For the skinned fiber experiments the relaxing solution and  
26 the  $\text{K}_2\text{SO}_4$ -based internal solution contained (mM) 125 K-glutamate, 10 HEPES, 1 EGTA, 6  
27  $\text{MgCl}_2$ , 5  $\text{Na}_2\text{-ATP}$ , 10 Na-phosphocreatine, 10 glucose, 0.13  $\text{CaCl}_2$  and 95  $\text{K}_2\text{SO}_4$ , 10  
28 HEPES, 1 EGTA, 6  $\text{MgCl}_2$ , 5  $\text{Na}_2\text{-ATP}$ , 10 Na-phosphocreatine, 10 glucose, 0.13  $\text{CaCl}_2$ ,  
29 respectively. Both solutions also contained 8% dextran.  
30  
31  
32  
33  
34  
35  
36  
37  
38  
39  
40  
41  
42  
43  
44  
45  
46  
47  
48  
49  
50  
51  
52  
53  
54  
55  
56  
57

58 For voltage-clamp experiments the external solution contained (in mM) 140 TEA-  
59 methanesulfonate, 2.5  $\text{CaCl}_2$ , 2  $\text{MgCl}_2$ , 10 TEA-HEPES and 0.002 tetrodotoxin, pH 7.20. The  
60 internal-like solution contained (in mM): 120 K-glutamate, 5  $\text{Na}_2\text{-ATP}$ , 5.5  $\text{MgCl}_2$ , 5  $\text{Na}_2$ -  
phosphocreatine, and 5 HEPES adjusted to pH 7.20 with K-OH.

### *Statistics*

Least-squares fits were performed using a Marquardt-Levenberg algorithm routine included in

1  
2  
3 Microcal Origin. Unless otherwise specified, data values are presented as means  $\pm$  SE.

4  
5  
6 Statistical significance was determined using a Student's *t*-test assuming significance for  $p <$   
7  
8 0.05.  
9  
10  
11  
12  
13  
14  
15  
16  
17  
18  
19  
20  
21  
22  
23  
24  
25  
26  
27  
28  
29  
30  
31  
32  
33  
34  
35  
36  
37  
38  
39  
40  
41  
42  
43  
44  
45  
46  
47  
48  
49  
50  
51  
52  
53  
54  
55  
56  
57  
58  
59  
60

For Peer Review

## RESULTS

Fig. 1 shows strips from baseline corrected line-scan ( $x, t$ ) images of fluo-3 fluorescence taken from mouse and frog skeletal muscle fibers under different conditions. The image in Fig. 1 A was obtained from a chemically skinned mouse muscle fiber equilibrated with fluo-3. As originally reported by Kirsch et al. (2001) in mammalian muscle fibers, these conditions favor the occurrence of  $\text{Ca}^{2+}$  spark-like events. The first row in Table I gives mean values for standard parameters measured from 201 such events collected from 7 mouse fibers under these conditions. Values are in agreement with those reported previously by Kirsh et al. (2001), Zhou et al. (2003) and Szentesi et al. (2004) in chemically skinned mammalian muscle fibers. Fig. 1 B is simply presented as an illustrative example of the fact that qualitatively similar events can be recorded from skinned frog muscle fibers under these same conditions. Fig. 1 C and D were obtained from a mouse skeletal muscle fiber under silicone voltage-clamp conditions; the fiber was depolarized by a 500 ms long step to  $-45$  mV (C) and to  $-40$  mV (D), starting 200 ms after the beginning of the line-scan. As previously observed in either mechanically dissected (Shirokova et al., 1998) or enzymatically dissociated (Csernoch et al., 2004) rat muscle fibers under vaseline-gap voltage-clamp conditions, the depolarization induced a diffuse increase in fluorescence, out of which there was no sign of spark-like  $\text{Ca}^{2+}$  release events. Conversely, when such measurements were achieved on frog muscle fibers, membrane depolarization elicited unmistakable  $\text{Ca}^{2+}$  sparks, the frequency of which increased with the amplitude of the pulse, as illustrated in Fig. 1 E-F. Mean values for parameters measured from such voltage-activated sparks in 5 frog fibers under these conditions are given in the third row of Table I; they fit reasonably well within the range of parameters reported by others in frog muscle fibers voltage-clamped with the vaseline-gap technique (see e.g. Table 2 from Baylor, 2005). When compared to the values from the sparks detected here in skinned

1  
2  
3 mouse fibers, voltage-activated sparks from frog fibers yielded a definitely shorter duration  
4  
5 whereas their amplitude and FWHM were very similar to the values in the skinned mouse  
6  
7 fibers. Overall, these data establish the reliability of our system and conditions in regard to the  
8  
9 possibility of detecting elementary  $\text{Ca}^{2+}$  release events in isolated skeletal muscle fibers.

10  
11 Our goal then was to track elementary events within the images collected from intact voltage-  
12  
13 clamped mouse muscle fibers. The images in Fig. 2 illustrate the strategy that was used. Fig. 2  
14  
15 A shows a raw line-scan image of the fluo-3 fluorescence obtained in response to a 500 ms  
16  
17 long depolarization to -50 mV. The image was baseline corrected (Fig. 2 B) and filtered in the  
18  
19 spatial domain (Fig. 2 C) as described in Methods. Notice that the time course of the spatially  
20  
21 averaged global  $F/F_0$  signal is shown at the bottom of Fig. 2 B. The filtering procedure  
22  
23 removed the diffuse continuous increase in fluorescence, clearly revealing the presence of  
24  
25 local stripes of elevated fluorescence intensity within the depolarization interval. Fig. 2 D  
26  
27 shows the corresponding created binary image in which all pixels with values lower than the  
28  
29 threshold level were set to zero while other pixel values were set to unity. The threshold was  
30  
31 set to twice the standard deviation of the background signal. This procedure highlighted two  
32  
33 main regions (*a* and *b*) within the image, at *x* locations pointed by an arrow. The time course  
34  
35 of the corresponding signals is shown superimposed on the image in Fig. 2 C. Notice that in  
36  
37 this example these regions were already quite well discernible within the initial raw image,  
38  
39 which was not always the case. Within the present study, such supra-threshold local signals  
40  
41 were detected in 99 out of 204 images analyzed from 23 fibers. The areas containing the local  
42  
43 signals were excised from the filtered image shown in Fig. 2 C and then analyzed separately  
44  
45 to determine their morphological properties. Fig. 3 shows examples of three such identified  
46  
47 events within another processed line-scan image. Fig. 3 A shows the baseline corrected image  
48  
49 and Fig. 3 B the corresponding filtered image. The time course of each event is shown  
50  
51 superimposed on the image in Fig. 3 B with an arrow pointing to its corresponding location.  
52  
53  
54  
55  
56  
57  
58  
59  
60

1  
2  
3 The amplitude of these local fluorescence changes was small, around  $0.2 F_0$ . Their time  
4  
5 course was either quite simple, roughly corresponding to a step-like change in fluorescence  
6  
7 (as for the event in the middle of the image) or appeared more complex with features that may  
8  
9 be thought to reflect the presence of amplitude sub-levels or closures and re-openings (see  
10  
11 also Fig. 4). However, within the present study, events were defined and quantitatively  
12  
13 characterized in the simplest way (see Methods) and no attempt was done to apprehend any  
14  
15 further intrinsic complexity. It should also be stressed that under our conditions the large  
16  
17 majority of the detected events occurred during the depolarization interval. In some rare cases,  
18  
19 however, we could also observe local signals likely to result from the re-opening of the  
20  
21 channel (or group of channels) responsible for this type of activity after the end of the  
22  
23 depolarization, as shown in Fig. 4 A- B. Six such post-pulse events were detected in the 99  
24  
25 total number of images where events activated during a depolarization were identified. These  
26  
27 events were not included in the analysis. In Fig. 3, the inset on the right shows the spatial  
28  
29 profile of the event with the time course shown in the middle of the image. The profile was  
30  
31 well fitted by a Gaussian function, the result of which is shown superimposed on the data  
32  
33 points. Mean values for the amplitude, duration and FWHM obtained from events identified  
34  
35 in  $(x, t)$  images collected under these conditions (that is in response to 500 ms long  
36  
37 depolarizing pulses irrespective of the depolarization level) are reported in Table I, while  
38  
39 corresponding distribution histograms are presented in Fig. 5. The spatio-temporal properties  
40  
41 of these events are very different from those of both the spontaneous  $Ca^{2+}$  sparks from  
42  
43 skinned mouse fibers and the voltage-activated  $Ca^{2+}$  sparks in frog fibers: the mean values for  
44  
45 amplitude and FWHM of the voltage-activated mouse events were about one fifth and twice  
46  
47 the corresponding values from the  $Ca^{2+}$  sparks, respectively. The mean duration of the  
48  
49 voltage-activated mouse events was much larger than that of both types of  $Ca^{2+}$  sparks;  
50  
51 furthermore, as shown in Fig. 5 C, the distribution of event duration was broad and yielded a  
52  
53  
54  
55  
56  
57  
58  
59  
60

1  
2  
3  
4  
5  
6  
7  
8  
9  
10  
11  
12  
13  
14  
15  
16  
17  
18  
19  
20  
21  
22  
23  
24  
25  
26  
27  
28  
29  
30  
31  
32  
33  
34  
35  
36  
37  
38  
39  
40  
41  
42  
43  
44  
45  
46  
47  
48  
49  
50  
51  
52  
53  
54  
55  
56  
57  
58  
59  
60

peak for duration values close to 500 ms which corresponds to the duration of the voltage clamp depolarization. Very few events of longer duration could be detected under these conditions, suggesting that events tended to be terminated by membrane repolarization. This was confirmed by examining the duration of events triggered by membrane depolarization of 200 ms and 800 ms duration. Fig. 6 A-C presents pairs of corresponding baseline corrected- (left) and processed- (right) line-scan images taken while a voltage-clamp depolarization of 200 ms, 500 ms and 800 ms duration was applied, respectively. The time course of a detected event is shown superimposed to each processed image. There was a clear dependence of the event duration upon the length of the pulse as also quantitatively illustrated in Fig. 6 D where the mean values for the event duration are plotted *versus* the pulse duration. In order to highlight the variability of the event duration the error bars in Fig. 6 D correspond to the standard deviation of the mean values.

Assuming that the discrete fluorescence signals detected here correspond to voltage-activated elementary  $\text{Ca}^{2+}$  release events, we attempted to reconstruct the corresponding time course of global  $\text{Ca}^{2+}$  influx into the myoplasm from the distribution of the events amplitude and duration shown in Fig. 5. This calculation is based on the simple concept that, for a  $\text{Ca}^{2+}$  influx to be operating, a  $\text{Ca}^{2+}$  channel needs to be open and to have not yet closed. The time-course of the probability for channels to be open is given by the cumulative distribution of latencies of the events (Fig. 7 A) whereas the time course of the probability that a channel gets closed is derived from the cumulative distribution of duration of the events (Fig. 7 B). The resulting time course of global  $\text{Ca}^{2+}$  influx, calculated as the product of the two, is shown in Fig. 7 C. Interestingly this time course resembles the one that one can calculate from the average macroscopic fluo-3 fluorescence transient obtained from the same images, using a modeling approach taking into account the known properties of the myoplasmic  $\text{Ca}^{2+}$  removal

1  
2  
3 processes in this preparation (Szentesi et al., 2001). The two methods provided a  $\text{Ca}^{2+}$  flux  
4  
5 that rose to a somewhat steady level and exhibited no, or very small early peak.  
6  
7  
8  
9

10  
11 In order to further establish the importance of membrane repolarization in the termination of  
12 the discrete fluorescence signals detected here line-scan images were recorded in voltage-  
13 clamped fibers pressure-micro-injected with the scorpion toxin maurocalcine. In an earlier  
14 study we demonstrated that this toxin affects the voltage-activated global  $\text{Ca}^{2+}$  transient in a  
15 way suggesting that it binds to  $\text{Ca}^{2+}$  release channels opened by the membrane depolarization  
16 and prevents them from closing upon membrane repolarization (Pouvreau et al., 2006). Fig. 8  
17  
18 *A-B* shows  $(x, t)$  fluo-3 fluorescence images taken from two separate mouse muscle fibers  
19 injected with maurocalcine and depolarized by a 200 ms long pulse. The figure shows both  
20 the baseline corrected images (left) and the corresponding processed images (right). **The trace**  
21 **below each baseline corrected image shows the corresponding spatially averaged global  $F/F_0$**   
22 **signal.** The images contained discrete fluorescence events that started during the  
23 depolarization and ran all the way through the recording period. The time course of two such  
24 events is shown superimposed on the filtered images. They yielded an amplitude similar to  
25 that of events detected under control conditions. A total of 15  $(x, t)$  images containing  
26 suprathreshold events were collected from 7 voltage-clamped fibers injected with  
27 maurocalcine. Both non-ending events resembling those shown in Fig. 8 *A-B* and events  
28 similar to those observed in control fibers could be detected. The graph in Fig. 8 *C* presents  
29 the dependence of the individual values for the duration of the detected events in  
30 maurocalcine-injected fibers (open circles) *versus* the length of the pulse. Events that did not  
31 end over the recorded period were arbitrarily assumed to have stopped at the end of the record  
32 (1.38 s following the beginning of the pulse). The mean values obtained from control fibers  
33 (filled circles, Fig. 6 *D*) are also shown for comparison. In the presence of maurocalcine 11  
34  
35  
36  
37  
38  
39  
40  
41  
42  
43  
44  
45  
46  
47  
48  
49  
50  
51  
52  
53  
54  
55  
56  
57  
58  
59  
60

1  
2  
3  
4  
5  
6  
7  
8  
9  
10  
11  
12  
13  
14  
15  
16  
17  
18  
19  
20  
21  
22  
23  
24  
25  
26  
27  
28  
29  
30  
31  
32  
33  
34  
35  
36  
37  
38  
39  
40  
41  
42  
43  
44  
45  
46  
47  
48  
49  
50  
51  
52  
53  
54  
55  
56  
57  
58  
59  
60

suprathreshold non-ending events were detected. Corresponding mean values for spatial half-width and amplitude were  $1.47 \pm 0.09 \mu\text{m}$  and  $0.15 \pm 0.02 \Delta F/F_0$ , respectively. Fig. 9 shows mean values for the average amplitude and FWHM of these 11 events when measured during the depolarizing pulse (during step) and after the pulse (after step). Overall, the amplitude and FWHM were not significantly affected by membrane repolarization.

For Peer Review

## DISCUSSION

The search for the elementary components that build up the global cytoplasmic  $\text{Ca}^{2+}$  transient responsible for the contraction of mammalian skeletal muscle fibers is on. While in frog fibers the voltage-activated elementary SR  $\text{Ca}^{2+}$  release events (the  $\text{Ca}^{2+}$  sparks) have been extensively characterized, detection of the corresponding events in mammalian muscle fibers is proving to be a much more challenging task. Indeed, irrespective of the experimental system used, it seems that frog muscle fibers always produce  $\text{Ca}^{2+}$  sparks in response to membrane depolarization (see for review Baylor, 2005). On the contrary and unexpectedly, the first voltage-clamped mammalian muscle fibers (rat cut fibers handled with the vaseline-gap technique) that were reported to be held under a confocal microscope proved incapable of generating such events (Shirokova et al., 1998). This definitely highlighted the possibility for major differences in the physiological mechanisms that control SR  $\text{Ca}^{2+}$  release between the two species.

We demonstrate here that this difference also holds true between intact enzymatically isolated frog and mouse muscle fibers held under silicone voltage-clamp conditions. In our hands, frog fibers generate  $\text{Ca}^{2+}$  sparks in response to membrane depolarization, with properties similar to those described in previous studies, while mouse fibers are endowed with a diffuse increase in the calcium-dye fluorescence devoid of typical sparks. This latter observation is thus consistent with the data obtained in rat cut fibers by Shirokova et al. (Shirokova et al., 1998). Using the vaseline-gap technique Csernoch et al. (2004) showed that spatially restricted discrete fluorescence signals of smaller amplitude and longer duration than sparks, could be detected in the rat fibers during voltage-clamp depolarizations. These signals yielded morphological properties similar to the so-called “embers” originally described by Gonzalez et al. (2000) in amphibian and by Kirsch et al. (2001) in skinned mammalian

1  
2  
3  
4  
5  
6  
7  
8  
9  
10  
11  
12  
13  
14  
15  
16  
17  
18  
19  
20  
21  
22  
23  
24  
25  
26  
27  
28  
29  
30  
31  
32  
33  
34  
35  
36  
37  
38  
39  
40  
41  
42  
43  
44  
45  
46  
47  
48  
49  
50  
51  
52  
53  
54  
55  
56  
57  
58  
59  
60

muscle fibers, and believed to result from the activity of either one or of a restricted number of highly synchronized RyRs (see Zhou et al., 2003; Szentesi et al., 2004). Here we also demonstrate that discrete local elevations of fluorescence can also be identified within the diffuse fluo-3 fluorescence increase triggered by a voltage-clamp depolarization in intact mouse muscle fibers. These signals also exhibit morphological properties close to those of embers. If compared to those observed in rat cut fibers by Csernoch et al (2004), the present events yield a somewhat smaller average amplitude (0.16 *versus* 0.19) and larger spatial half-width (2  $\mu\text{m}$  *versus* 1.3  $\mu\text{m}$ ). Given, however, the numerous differences between the two studies including the species and muscle type and the use of cut *versus* intact fibers we believe that the two sets of data agree remarkably well. Our results thus definitely establish these voltage-activated low amplitude long-lasting events as inherent components of the excitation-contraction coupling process of mammalian muscle. It should be stressed that, due in particular to their very low amplitude and to the presence of a concomitant diffuse increase in fluorescence, the study of these events proved to be much more difficult than that of voltage-activated  $\text{Ca}^{2+}$  release events (the sparks) in frog muscle. For instance, we have so far been unable to derive a voltage-dependence for the parameters of these events because of two main limitations. For once, fibers were injected with a solution that did not contain EGTA, or any other calcium buffer, apart from the dye itself; therefore, increasing the level of step depolarization rapidly tended to initiate the contraction of the fiber, resulting in the distortion of the images and rendering a reliable analysis impossible. In addition, the larger the level of depolarization the greater was the increase in the background fluorescence, which inescapably made the detection of the events ever more difficult. Nonetheless, in an attempt to crudely explore the voltage dependence, events measured at the most negative and positive membrane depolarization levels were grouped and the characteristic parameters for each group were determined. There was no difference in the mean amplitude of the events ( $0.152 \pm 0.010$ )

1  
2  
3 *versus*  $0.154 \pm 0.010$ ;  $n = 19$ ) between the two groups whereas there was a slight, but  
4  
5 statistically not significant, decrease in the latency for events detected at the largest  
6  
7 depolarization levels ( $109 \pm 32$  *versus*  $81 \pm 31$  ms), in line with the expectations. The fact that  
8  
9 the change in latency did not prove to be significant most likely results from the fact that  
10  
11 measurements at different voltages were conducted, due to the above mentioned reasons, on  
12  
13 different fibers. The inability to reliably detect events for large depolarizing levels led to  
14  
15 another somewhat frustrating issue that we could not demonstrate a statistically significant  
16  
17 increase in the frequency of events *versus* voltage, as was also the case in the preceding study  
18  
19 on rat fibers under vaseline-gap voltage-clamp conditions (Csernoch et al., 2004). Although  
20  
21 this is a critical aspect of the problem, it is quite clear that the conditions for triggering and/or  
22  
23 detecting these events will need to be improved before their voltage dependence can be  
24  
25 explored in detail. Along this line, we did make attempts to improve the detection by testing  
26  
27 other experimental conditions including the use of a high concentration of EGTA in the fibers  
28  
29 or the use of the calcium dye fluo-4 in place of fluo-3 (not illustrated). These conditions did  
30  
31 not provide sufficient improvement to help unravel the voltage dependence of the event  
32  
33 frequency.

34  
35 In any case we demonstrate that for a given depolarizing pulse length, the distribution  
36  
37 of the duration of these events exhibits a clear peak at values which correspond to the time of  
38  
39 repolarization of the membrane. This suggests that the channel activity underlying these  
40  
41 events tends to be shut by membrane repolarization. This is also confirmed by the strong  
42  
43 dependence of the mean event duration upon the depolarizing pulse length. This makes these  
44  
45 events good candidates to represent at least one class of voltage-activated SR  $\text{Ca}^{2+}$  release  
46  
47 events. Taken together these observations also indicate that the DHPR in its resting state, i.e.  
48  
49 when the T-tubular membrane potential is at its resting (-80 to -90 mV) value, exerts a tonic  
50  
51 inhibitory effect on the RyR. This would explain why intact mammalian fibers hardly produce  
52  
53  
54  
55  
56  
57  
58  
59  
60

1  
2  
3  
4  
5  
6  
7  
8  
9  
10  
11  
12  
13  
14  
15  
16  
17  
18  
19  
20  
21  
22  
23  
24  
25  
26  
27  
28  
29  
30  
31  
32  
33  
34  
35  
36  
37  
38  
39  
40  
41  
42  
43  
44  
45  
46  
47  
48  
49  
50  
51  
52  
53  
54  
55  
56  
57  
58  
59  
60

spontaneous events (Conklin et al., 1999; Chun et al., 2003; Zhou et al., 2003) whereas fibers with disrupted surface- and T-tubular membranes do so (Kirsch et al., 2001; Zhou et al., 2003; Isaeva et al., 2005). This concept is also in line with earlier findings on cultured mammalian myotubes where a spatially segregated voltage-controlled  $\text{Ca}^{2+}$  release devoid of discrete events and spontaneous  $\text{Ca}^{2+}$  release in the form of  $\text{Ca}^{2+}$  sparks, was demonstrated (Shirokova et al., 1999) and attributed later to the presence or absence of properly developed T-tubules and DHPR-RyR interactions (Zhou et al., 2006). It should be stressed, however, that the picture for the control of elementary calcium release events in mammals is far from being so clear. In the above framework any intervention that removes the inhibition exerted by the DHPR should favor the appearance of spontaneous events. This is clearly questioned, since neither chronic depolarization nor the presence of dihydropyridines, both favoring the transition to the inactivated state of the DHPR, provokes such events (Szappanos et al., 2005 and unpublished data), unless the inactivated state of the DHPR is also associated with a tonic inhibitory interaction between the voltage sensor and the calcium release channel.

We also found that the re-construction of the global  $\text{Ca}^{2+}$  release waveform from the elementary properties of these events was very much consistent with the waveform calculated from the average macroscopic change in fluo-3 fluorescence using a classical model of intracellular  $\text{Ca}^{2+}$  redistribution. Noticeably, both approaches provided a time course that rose monotonically and which did not display an early peak, suggesting that calcium-dependent inactivation did not play an important role at these low levels of activation. Future investigation of the properties of the events under conditions allowing application of more depolarized voltages will certainly provide further insights into this aspect of the regulation of the  $\text{Ca}^{2+}$  release channels.

Finally, we demonstrate that in the presence of maurocalcine, a specific sub-set of events could be detected that had a similar amplitude and spatial profile as those in control,

1  
2  
3 but were not terminated by membrane repolarization and had durations exceeding 1 s. Such  
4  
5 events were never observed under control conditions and should not be confused with the rare  
6  
7 examples of post-pulse events illustrated in Fig. 4 A-B which are likely to witness a channel  
8  
9 re-opening after the end of the pulse. Since maurocalcine was reported to induce long-lasting  
10  
11 subconductance states on isolated RyRs incorporated into lipid bilayers (Fajloun et al., 2000;  
12  
13 Esteve et al., 2003) and to evoke ember-like  $\text{Ca}^{2+}$  release events with long duration  
14  
15 (Szappanos et al., 2005), the events captured here should also correspond to channels  
16  
17 modified by the peptide. In addition, using global  $\text{Ca}^{2+}$  measurements we previously provided  
18  
19 data suggesting that, within the physiological functional frame of e-c coupling, maurocalcine  
20  
21 binds to RyR channels that open during membrane depolarization and that maurocalcine-  
22  
23 modified channels fail to close upon membrane repolarization (Pouvreau et al., 2006). We  
24  
25 believe that the non-ending events observed here provide a remarkable correlate for this  
26  
27 scheme, at the elementary level. Such events are indeed more than likely to correspond to the  
28  
29 activity of a single maurocalcine-bound RyR that is maintained open despite membrane  
30  
31 repolarization. It should be stressed that the possibility of two release channels binding  
32  
33 maurocalcine either at the same time or in close succession, has to be extremely low. The  
34  
35 observation that the parameters of the events are independent of whether they are measured  
36  
37 during or after the pulse also strongly argues in favor of the same channel being responsible  
38  
39 for the entire event. This, together with the fact that these events do not dramatically differ in  
40  
41 size from those measured under control conditions, render the possibility that the control  
42  
43 events are also generated by a single calcium release channel extremely likely. One should,  
44  
45 however, stress that if a group of channels, due to allosteric interactions, always gates  
46  
47 synchronously (as proposed by Marx et al., 1998), the present method would recognize them  
48  
49 as a single entity. Nevertheless, further in depth study of this effect of maurocalcine should  
50  
51 provide interesting clues regarding the control of the RyR channel activity.  
52  
53  
54  
55  
56  
57  
58  
59  
60

1  
2  
3  
4  
5  
6  
7  
8  
9  
10  
11  
12  
13  
14  
15  
16  
17  
18  
19  
20  
21  
22  
23  
24  
25  
26  
27  
28  
29  
30  
31  
32  
33  
34  
35  
36  
37  
38  
39  
40  
41  
42  
43  
44  
45  
46  
47  
48  
49  
50  
51  
52  
53  
54  
55  
56  
57  
58  
59  
60

Overall the present results provide definite additional insights into the *in vivo* function of the SR  $\text{Ca}^{2+}$  release channels in mammalian muscle. Although there is still a number of questions open, including for instance the mechanism underlying the diffuse increase in fluorescence observed during a depolarizing pulse, the present approach should prove useful to further characterize SR  $\text{Ca}^{2+}$  release under normal and stress or diseased conditions in mammalian muscle.

For Peer Review

## ACKNOWLEDGEMENTS

This work was supported by grants from CNRS, University Claude Bernard Lyon 1, Association Française contre les Myopathies, the Hungarian National Science Fund (OTKA T049151) and the French-Hungarian Balaton program.

For Peer Review

## REFERENCES

- 1  
2  
3  
4  
5  
6  
7  
8 Baylor, S. M. 2005. Calcium sparks in skeletal muscle fibres. *Cell Calcium* 37:513-530.
- 9  
10 Berridge, M. J. 2006. Calcium microdomains: organization and function. *Cell Calcium*  
11  
12 40:405-412.
- 13  
14 Cheng, H., Song, L.S., Shirokova, N., Gonzalez, A., Lakatta, E. G., Rios, E., Stern, M. D.  
15  
16 1999. Amplitude distribution of calcium sparks in confocal images: theory and  
17  
18 studies with an automatic detection method. *Biophys. J.* 76:606-617.
- 19  
20 Chun, L. G., Ward, C. W., Schneider, M. F. 2003. Ca<sup>2+</sup> sparks are initiated by Ca<sup>2+</sup> entry  
21  
22 in embryonic mouse skeletal muscle and decrease in frequency postnatally. *Am. J.*  
23  
24 *Physiol. Cell Physiol.* 285:C686-C697.
- 25  
26 Collet, C., Allard, B., Tourneur, Y., Jacquemond, V. 1999. Intracellular calcium signals  
27  
28 measured with indo-1 in isolated skeletal muscle fibres from control and mdx mice.  
29  
30 *J. Physiol.* 520:417-429.
- 31  
32 Conklin, M. W., Barone, V., Sorrentino, V., Coronado, R. 1999. Contribution of  
33  
34 ryanodine receptor type 3 to Ca<sup>2+</sup> sparks in embryonic mouse skeletal muscle.  
35  
36 *Biophys. J.* 77:1394-1403.
- 37  
38 Csernoch, L. 2007. Sparks and embers of skeletal muscle: the exciting events of  
39  
40 contractile activation. *Pflugers Arch.* 454:869-878.
- 41  
42 Csernoch, L., Pouvreau, S., Jacquemond, V. 2006. Voltage activated calcium release  
43  
44 events in mouse skeletal muscle fibers. *Biophys J.* 90:326a.
- 45  
46 Csernoch, L., Zhou, J., Stern, M. D., Brum, G., Rios, E. 2004. The elementary events of  
47  
48 Ca<sup>2+</sup> release elicited by membrane depolarization in mammalian muscle. *J. Physiol.*  
49  
50 557:43-58.
- 51  
52  
53  
54  
55  
56  
57  
58  
59  
60

- 1  
2  
3 Estève, E., Smida-Rezgui, S., Sarkozi, S., Szegedi, C., Regaya, I., Chen, L., Altafaj, X.,  
4  
5 Rochat, H., Allen, P., Pessah, I. N., Marty, I., Sabatier, J. M., Jona, I., DeWaard, M.,  
6  
7 Ronjat, M. 2003. Critical amino acid residues determine the binding affinity and the  
8  
9  $\text{Ca}^{2+}$  release efficacy of maurocalcine in skeletal muscle cells. *J. Biol. Chem.*  
10  
11 278:37823–37831.  
12  
13  
14  
15 Fajloun, Z., Kharrat, R., Chen, L., Lecomte, C., Di Luccio, E., Bichet, D., El Ayeb, M.,  
16  
17 Rochat, H., Allen, P. D., Pessah, I. N., DeWaard, M., Sabatier, J. M. 2000. Chemical  
18  
19 synthesis and characterization of maurocalcine, a scorpion toxin that activates  $\text{Ca}^{2+}$   
20  
21 release channel/ryanodine receptors. *FEBS Lett.* 469:179–185.  
22  
23  
24  
25 Gonzalez, A., Kirsch, W. G., Shirokova, N., Pizarro, G., Stern, M. D., Rios, E. 2000. The  
26  
27 spark and its ember: separately gated local components of  $\text{Ca}^{2+}$  release in skeletal  
28  
29 muscle. *J. Gen. Physiol.* 115:139-158.  
30  
31  
32  
33  
34  
35  
36  
37  
38  
39  
40  
41  
42  
43  
44  
45  
46  
47  
48  
49  
50  
51  
52  
53  
54  
55  
56  
57  
58  
59  
60
- Isaeva, E.V., Shkry, V. M., Shirokova, N. 2005. Mitochondrial redox state and  $\text{Ca}^{2+}$   
sparks in permeabilized mammalian skeletal muscle. *J Physiol.* 565:855–872.
- Jacquemond, V. 1997. Indo-1 fluorescence signals elicited by membrane depolarization in  
enzymatically isolated mouse skeletal muscle fibers. *Biophys. J.* 73:920-928.
- Kirsch, W.G., Uttenweiler, D., Fink, R. H.. 2001. Spark- and ember-like elementary  $\text{Ca}^{2+}$   
release events in skinned fibres of adult mammalian skeletal muscle. *J. Physiol.*  
537:379-389.
- Klein, M.G., Cheng, H., Santana, L. F., Jiang, Y. H., Lederer, W. J., Schneider, M. F.  
1996. Two mechanisms of quantized calcium release in skeletal muscle. *Nature*  
379:455-458.
- Klein, M.G., Schneider, M. F. 2006.  $\text{Ca}^{2+}$  sparks in skeletal muscle. *Prog. Biophys. Mol.*  
*Biol.* 92:308-332.

- 1  
2  
3 Marx, S.O., Ondrias, K., Marks, A. R. 1998. Coupled gating between individual muscle  
4  
5  $\text{Ca}^{2+}$  release channels (ryanodine receptors). *Science* 281:818–821.  
6  
7  
8  
9  
10  
11  
12  
13  
14  
15  
16  
17  
18  
19  
20  
21  
22  
23  
24  
25  
26  
27  
28  
29  
30  
31  
32  
33  
34  
35  
36  
37  
38  
39  
40  
41  
42  
43  
44  
45  
46  
47  
48  
49  
50  
51  
52  
53  
54  
55  
56  
57  
58  
59  
60
- Pouvreau, S., Csernoch, L., Allard, B., Sabatier, J. M., De Waard, M., Ronjat, M.,  
Jacquemond, V. 2006. Transient loss of voltage control of  $\text{Ca}^{2+}$  release in the  
presence of maurocalcine in skeletal muscle. *Biophys. J.* 91:2206-2215.
- Pouvreau, S., Royer, L., Yi, J., Brum, G., Meissner, G., Rios, E., Zhou, J. 2007.  $\text{Ca}^{2+}$   
sparks operated by membrane depolarization require isoform 3 ryanodine receptor  
channels in skeletal muscle. *Proc. Natl. Acad. Sci. USA.* 104:5235-5240.
- Shirokova, N., Garcia, J., Rios, E. 1998. Local calcium release in mammalian skeletal  
muscle. *J. Physiol.* 512:377-384.
- Shirokova, N, Shirokov, R., Rossi, D., Gonzalez, A., Kirsch, W. G., Garcia, J., Sorrentino,  
V., Rios, E. 1999. Spatially segregated control of  $\text{Ca}^{2+}$  release in developing skeletal  
muscle of mice. *J. Physiol.* 521:483-495.
- Szentesi, P., Collet, C., Sarközi, S., Szegedi, C., Jona, I., Jacquemond, V., Kovacs, L.,  
Csernoch, L. 2001. Effects of dantrolene on steps of excitation-contraction coupling  
in mammalian skeletal muscle fibers. *J. Gen. Physiol.* 118:355-375.
- Szentesi, P., Szappanos, H., Szegedi, C., Gönczi, M., Jona, I., Cseri, J., Kovacs, L.,  
Csernoch, L. 2004. Altered elementary calcium release events and enhanced calcium  
release by thymol in rat skeletal muscle. *Biophys. J.* 86:1436-1453.
- Szappanos, H, Smida-Rezgui, S., Cseri, J., Simut, C., Sabatier, J. M., De Waard, M.,  
Kovács, L., Csernoch, L., Ronjat, M. 2005. Differential effects of maurocalcine on  
 $\text{Ca}^{2+}$  release events and depolarization-induced  $\text{Ca}^{2+}$  release in rat skeletal muscle. *J.*  
*Physiol.* 565:843-853.
- Tsugorka, A., Rios, E., Blatter, L. A. 1995. Imaging elementary events of calcium release  
in skeletal muscle cells. *Science* 269:1723-1726.

1  
2  
3 Zhou, J., Brum, G., Gonzalez, A., Launikonis, B. S., Stern, M. D., Rios, E. 2003. Ca<sup>2+</sup>  
4 sparks and embers of mammalian muscle. Properties of the sources. *J. Gen. Physiol.*  
5  
6 122:95-114.  
7  
8

9  
10 Zhou, J., Yi, J., Royer, L., Launikonis, B. S., Gonzalez, A., Garcia, J., Rios, E. 2006. A  
11 probable role of dihydropyridine receptors in repression of Ca<sup>2+</sup> sparks demonstrated  
12 in cultured mammalian muscle. *Am. J. Physiol. Cell Physiol.* 290: C539-C553.  
13  
14  
15  
16  
17  
18  
19  
20  
21  
22  
23

24  
25  
26  
27  
28  
29  
30  
31  
32  
33  
34  
35  
36  
37  
38  
39  
40  
41  
42  
43  
44  
45  
46  
47  
48  
49  
50  
51  
52  
53  
54  
55  
56  
57  
58  
59  
60

For Peer Review

## FIGURE LEGENDS

**Figure 1. Spontaneous and voltage activated  $\text{Ca}^{2+}$  release events in skinned and intact skeletal muscle fibers, respectively.** *A, B*, strips of fluo-3 fluorescence line-scan images taken from a chemically skinned skeletal muscle fiber isolated from a mouse and from a frog, respectively. The frog image was from measurements performed in the Department of Physiology at University of Debrecen under the conditions described in Szentesi et al. (2004). *C, D*, strips of line-scan images from a voltage-clamped intact mouse skeletal muscle fiber depolarized by a 500 ms long pulse to -45 and -40 mV, respectively. *E, F* strips of line-scan images from a voltage-clamped intact frog skeletal muscle fiber depolarized by a 500 ms long pulse to -55 and -50 mV, respectively.

**Figure 2. Identification of voltage-activated calcium release events.** *A*, raw fluo-3 fluorescence line-scan image from a mouse skeletal muscle fiber. *B*, corresponding image after correction for baseline fluorescence ( $F/F_0$ ).  $F_0(x)$  was obtained by averaging the fluorescence in the time domain during the baseline period (200 ms). *The trace below the image shows the corresponding spatially averaged global  $F/F_0$  signal.* *C*, corresponding  $F/F_0$  image after high-pass FFT filtering (see Methods). *D*,  $\text{Ca}^{2+}$  release events identified by the detection routine; *the time course of the corresponding events is shown superimposed on the image in Fig. 2 C; it was obtained by averaging three neighboring lines in the space domain positioned at the center of the events.*

**Figure 3. Time course and spatial spread of voltage-evoked  $\text{Ca}^{2+}$  release events.** *A*, *baseline corrected fluo-3 fluorescence line-scan image from a mouse skeletal muscle fiber depolarized by a 500 ms long depolarization to -60 mV. The bottom trace shows the*

1  
2  
3 corresponding spatially averaged global  $F/F_0$  signal. *B*, corresponding  $F/F_0$  image after high-  
4 pass FFT filtering. Identified  $Ca^{2+}$  release events (as described in Fig. 2) were further analyzed  
5 by averaging three neighboring lines in the space domain, positioned at the center of the  
6 events (marked by arrows) to obtain their time course. The inset on the right shows the spatial  
7 spread of the event on the left in the line-scan image; the superimposed line corresponds to  
8 the result from fitting a Gaussian function to estimate FWHM.  
9  
10  
11  
12  
13  
14  
15  
16  
17  
18  
19

20 **Figure 4. Rarely observed non-standard events.** Strips of fluo-3 fluorescence line-scan  
21 images from two distinct mouse skeletal muscle fibers depolarized by a 500 ms long pulse. *A*  
22 and *C* show the baseline corrected fluorescence images; the corresponding spatially averaged  
23 global  $F/F_0$  signal is shown at the bottom. *B* and *D* show the corresponding filtered images.  
24 Fluorescence events suggesting RyR channels closure followed by re-opening were  
25 occasionally detected after (*A*, *B*) and during a depolarizing pulse (*C*, *D*). Such complex  
26 events were seen in 4 and 11 images, respectively, out of the total of 99 images where events  
27 were detected and analyzed.  
28  
29  
30  
31  
32  
33  
34  
35  
36  
37  
38  
39  
40  
41  
42

43 **Figure 5. Properties of voltage-evoked  $Ca^{2+}$  release events in mouse skeletal muscle**  
44 **fibers.** Event amplitude (*A*), latency (*B*), duration (*C*) and FWHM (*D*) are presented as  
45 distribution histograms.  
46  
47  
48  
49  
50  
51  
52

53 **Figure 6.  $Ca^{2+}$  release events for various durations of membrane depolarization.**

54 *A-C*, baseline corrected ( $F/F_0$ ) line-scan images of fluo-3 fluorescence (left) and  
55 corresponding filtered images (right, see Methods) from three distinct mouse skeletal muscle  
56 fibers depolarized by voltage-clamp pulses, In *A*, *B* and *C* the fiber was depolarized by a 200-,  
57 500- and 800 ms-long pulse from -80 mV to -30, -30 and -40 mV, respectively; the trace  
58  
59  
60

1  
2  
3 below each image corresponds to the spatially averaged global  $F/F_0$  signal. In the right panels  
4  
5 the traces show the time course of an identified  $Ca^{2+}$  release event (arrow) within each  
6  
7 corresponding image. *D*, dependence of the mean event duration upon the length of the pulse;  
8  
9 data are from 13, 121 and 15 events for pulses of 200, 500 and 800 ms duration, respectively.  
10  
11 Error bars correspond to the standard deviation.  
12  
13  
14  
15  
16

17  
18 **Figure 7. Reconstruction of the SR  $Ca^{2+}$  release flux.** *A, B*, cumulative distribution of  
19  
20 latencies ( $cD(lat)$ ) and of time to channel closure ( $cD(ttcc)$ ) from  $Ca^{2+}$  release events elicited  
21  
22 by 500 ms long depolarizations. *C*, time course of SR permeability calculated as  $cD(lat) \cdot (1 -$   
23  
24  $cD(ttcc))$ . *D*,  $Ca^{2+}$  release flux (open squares) estimated from the global calcium transient  
25  
26 obtained from averaging the  $F/F_0$  images in the spatial domain (thin line). Global  $Ca^{2+}$  release  
27  
28 was calculated using a removal model (see Szentesi et al., 2004).  
29  
30

31  
32 **Figure 8. Voltage-activated  $Ca^{2+}$  release events in the presence of Maurocalcine.**

33  
34 *A-B*, baseline corrected ( $F/F_0$ ) line-scan images of fluo-3 fluorescence (left) and  
35  
36 corresponding filtered images (right, see Methods) from two distinct mouse skeletal muscle  
37  
38 fibers depolarized by 200 ms long voltage-clamp pulses to -35 mV and -40 mV, respectively.  
39  
40 The two fibers were injected with a solution containing 0.5 mM maurocalcine (see Methods).  
41  
42 *C*, dependence of the values for the duration of the events in maurocalcine-injected fibers  
43  
44 (open circles) versus the length of the pulse; filled circles correspond to the mean values in  
45  
46 control fibers (see text for details).  
47  
48  
49  
50  
51  
52  
53  
54

55  
56 **Figure 9. Amplitude and duration of the  $Ca^{2+}$  release events non-interrupted by**  
57  
58 **membrane repolarization in the presence of Maurocalcine.** *A, B*, mean values for the  
59  
60 amplitude and FWHM of the events during and after the end of the depolarization ( $n=11$ ).

1  
2  
3  
4  
5  
6  
7  
8  
9  
10  
11  
12  
13  
14  
15  
16  
17  
18  
19  
20  
21  
22  
23  
24  
25  
26  
27  
28  
29  
30  
31  
32  
33  
34  
35  
36  
37  
38  
39  
40  
41  
42  
43  
44  
45  
46  
47  
48  
49  
50  
51  
52  
53  
54  
55  
56  
57  
58  
59  
60

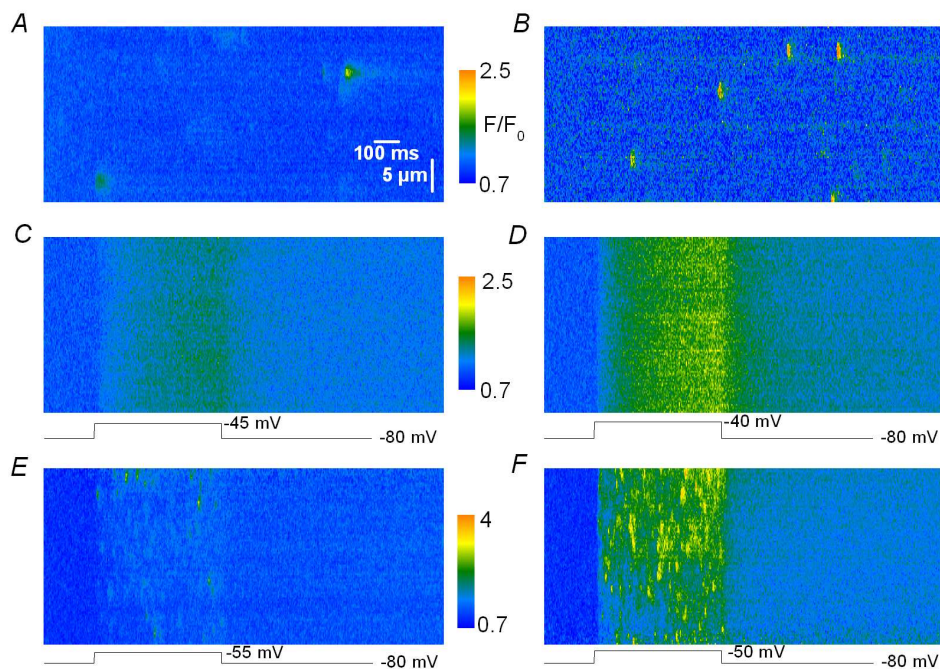
For Peer Review

TABLE I

*Average properties of calcium release events*

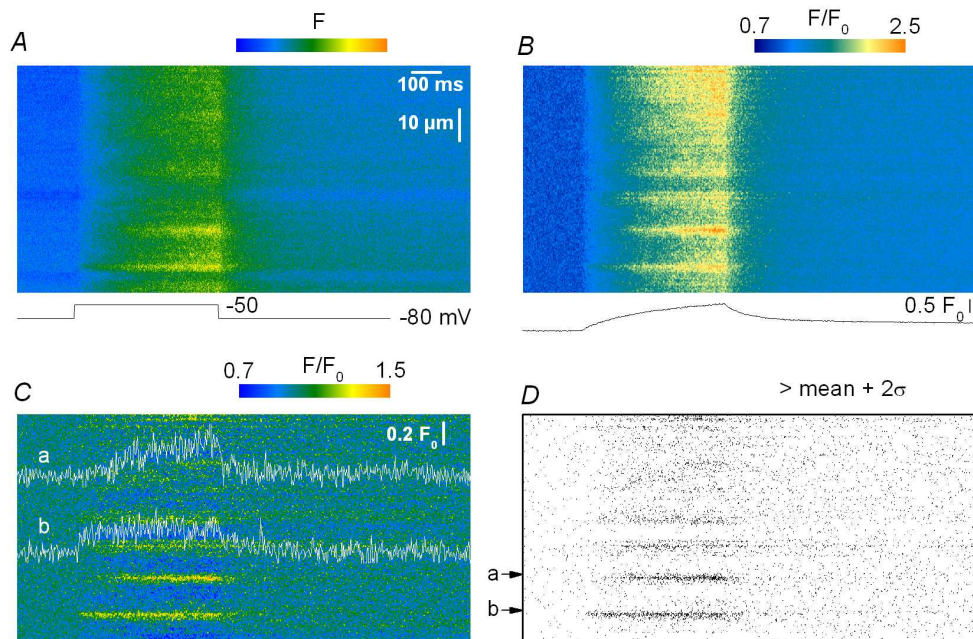
		<i>Amplitude</i>	<i>Full duration</i>	<i>FWHM</i>
		$(\Delta F/F_0)$	(ms)	( $\mu m$ )
	skinned ( $n=201$ )	$0.93 \pm 0.02$	$64.1 \pm 4.2$	$0.98 \pm 0.04$
mouse	voltage-activated <sup>a</sup> ( $n=123$ )	$0.16 \pm 0.005$	$383.8 \pm 18.1$	$1.93 \pm 0.1$
frog	voltage-activated* ( $n=115$ )	$1.00 \pm 0.05$	$13.4 \pm 0.53$	$0.90 \pm 0.02$

<sup>a</sup>Voltage-evoked events were detected using 500 ms long depolarizing pulses



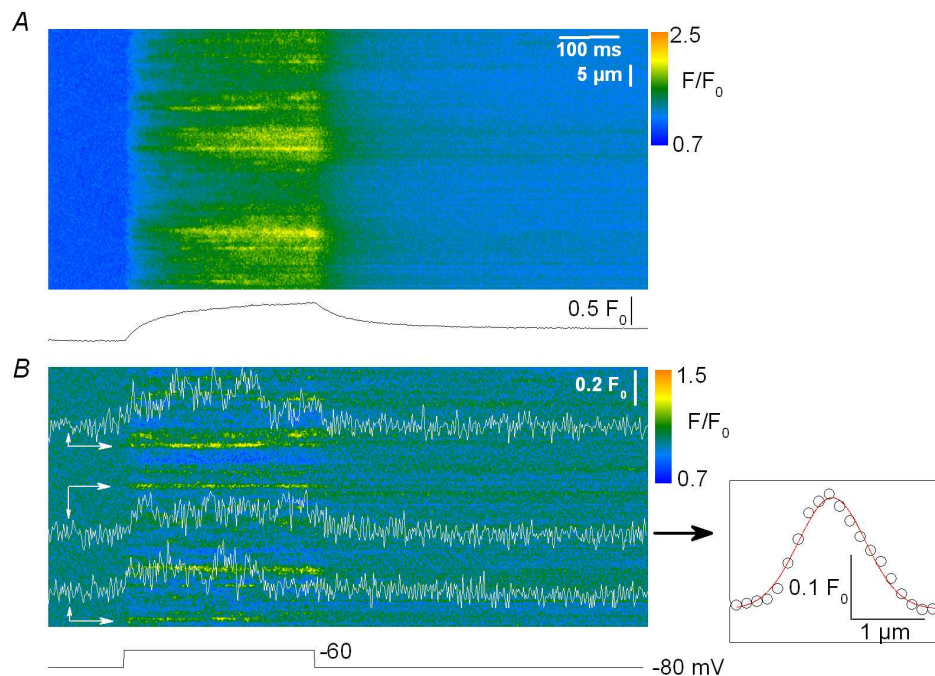
Spontaneous and voltage activated Ca<sup>2+</sup> release events in skinned and intact skeletal muscle fibers, respectively. A, B, strips of fluo-3 fluorescence line-scan images taken from a chemically skinned skeletal muscle fiber isolated from a mouse and from a frog, respectively. The frog image was from measurements performed in the Department of Physiology at University of Debrecen under the conditions described in Szentesi et al. (2004). C, D, strips of line-scan images from a voltage-clamped intact mouse skeletal muscle fiber depolarized by a 500 ms long pulse to -45 and -40 mV, respectively. E, F strips of line-scan images from a voltage-clamped intact frog skeletal muscle fiber depolarized by a 500 ms long pulse to -55 and -50 mV, respectively.

286x201mm (150 x 150 DPI)



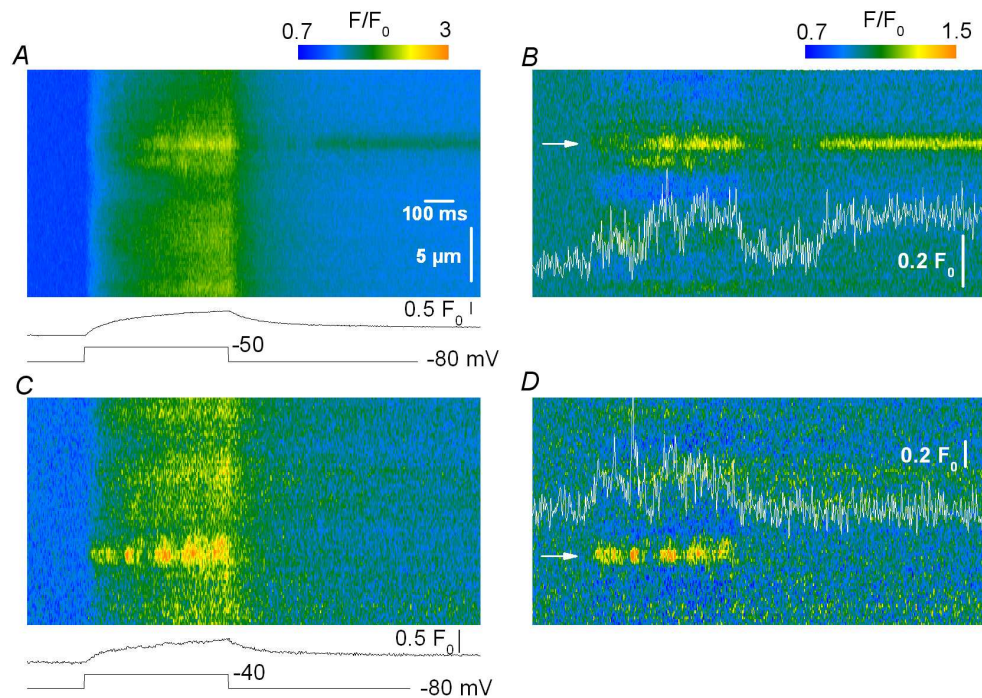
A, raw fluo-3 fluorescence line-scan image from a mouse skeletal muscle fiber. B, corresponding image after correction for baseline fluorescence ( $F/F_0$ ).  $F_0(x)$  was obtained by averaging the fluorescence in the time domain during the baseline period (200 ms). The trace below the image shows the corresponding spatially averaged global  $F/F_0$  signal. C, corresponding  $F/F_0$  image after high-pass FFT filtering (see Methods). D,  $\text{Ca}^{2+}$  release events identified by the detection routine; the time course of the corresponding events is shown superimposed on the image in Fig. 2 C; it was obtained by averaging three neighboring lines in the space domain positioned at the center of the events.

286x201mm (150 x 150 DPI)



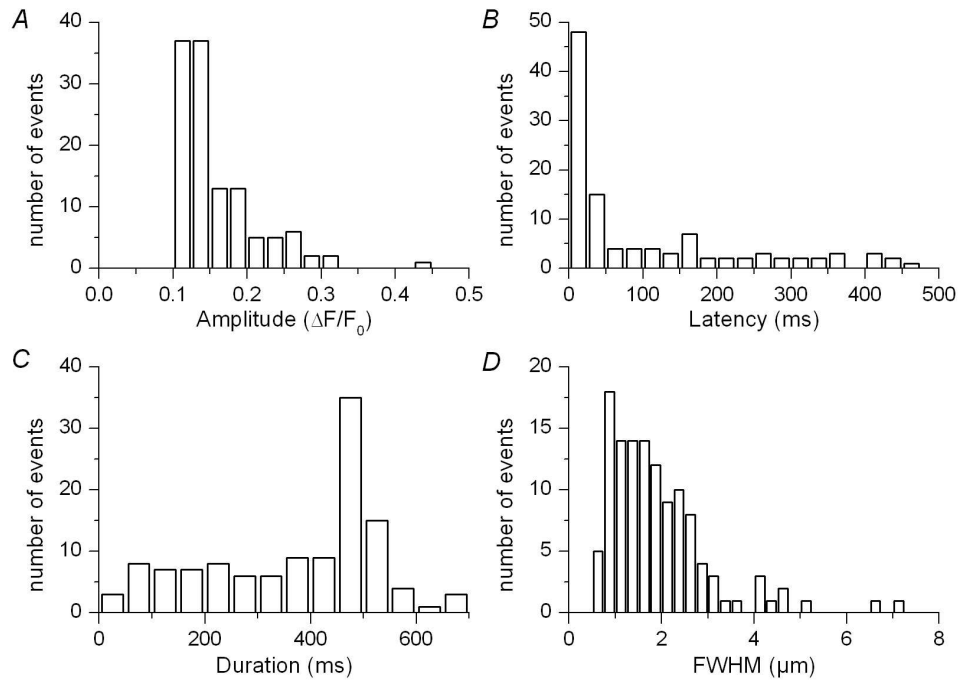
Time course and spatial spread of voltage-evoked  $\text{Ca}^{2+}$  release events. **A**, baseline corrected fluo-3 fluorescence line-scan image from a mouse skeletal muscle fiber depolarized by a 500 ms long depolarization to  $-60$  mV. The bottom trace shows the corresponding spatially averaged global  $F/F_0$  signal. **B**, corresponding  $F/F_0$  image after high-pass FFT filtering. Identified  $\text{Ca}^{2+}$  release events (as described in Fig. 2) were further analyzed by averaging three neighboring lines in the space domain, positioned at the center of the events (marked by arrows) to obtain their time course. The inset on the right shows the spatial spread of the event on the left in the line-scan image; the superimposed line corresponds to the result from fitting a Gaussian function to estimate FWHM.

286x201mm (150 x 150 DPI)



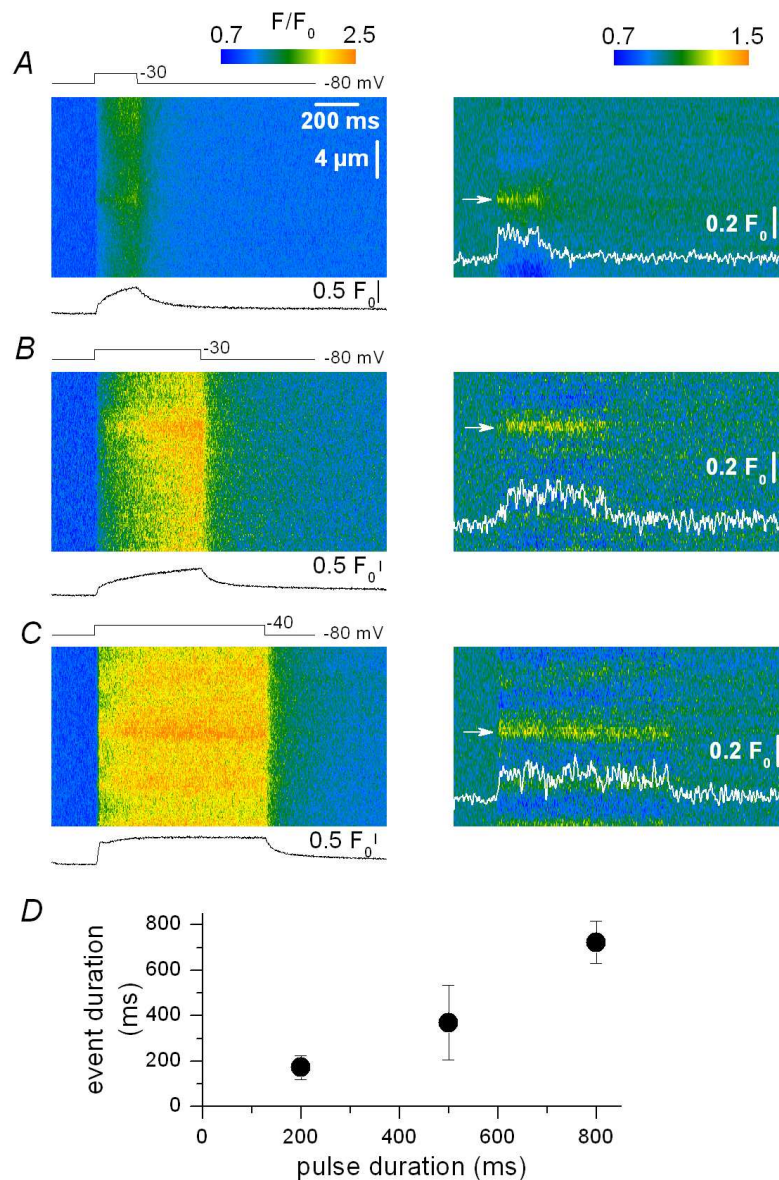
Rarely observed non-standard events. Strips of fluo-3 fluorescence line-scan images from two distinct mouse skeletal muscle fibers depolarized by a 500 ms long pulse. A and C show the baseline corrected fluorescence images; the corresponding spatially averaged global  $F/F_0$  signal is shown at the bottom. B and D show the corresponding filtered images. Fluorescence events suggesting RyR channels closure followed by re-opening were occasionally detected after (A, B) and during a depolarizing pulse (C, D). Such complex events were seen in 4 and 11 images, respectively, out of the total of 99 images where events were detected and analyzed.

286x201mm (150 x 150 DPI)



Properties of voltage-evoked  $\text{Ca}^{2+}$  release events in mouse skeletal muscle fibers. Event amplitude (A), latency (B), duration (C) and FWHM (D) are presented as distribution histograms.

286x201mm (150 x 150 DPI)



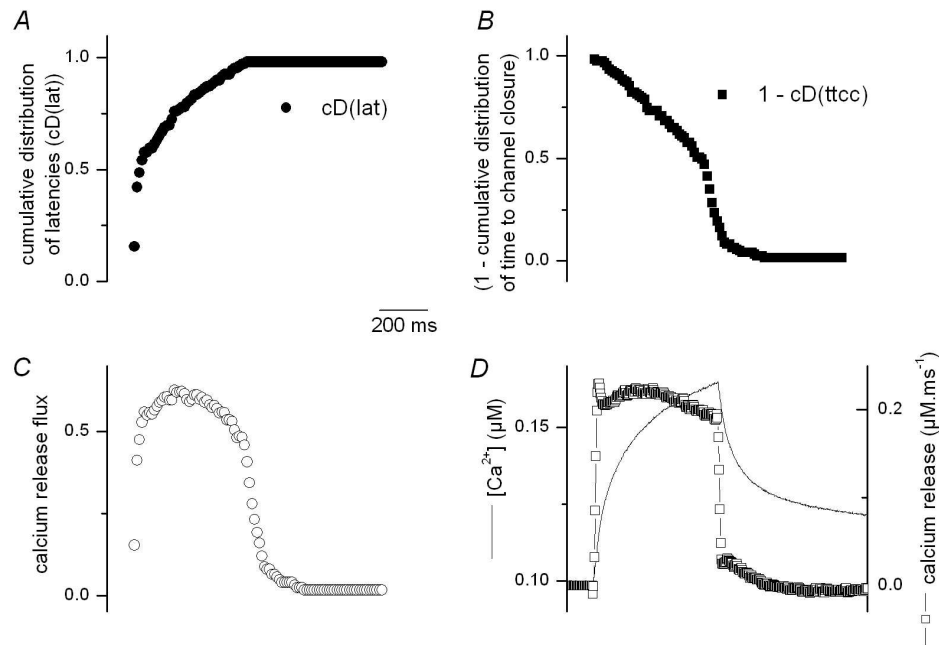
Ca<sup>2+</sup> release events for various durations of membrane depolarization. A-C, baseline corrected (F/F<sub>0</sub>) line-scan images of fluo-3 fluorescence (left) and corresponding filtered images (right, see Methods) from three distinct mouse skeletal muscle fibers depolarized by voltage-clamp pulses. In A, B and C the fiber was depolarized by a 200-, 500- and 800 ms-long pulse from -80 mV to -30, -30 and -40 mV, respectively; the trace below each image corresponds to the spatially averaged global F/F<sub>0</sub> signal. In the right panels the traces show the time course of an identified Ca<sup>2+</sup> release event (arrow) within each corresponding image. D, dependence of the mean event duration upon the

1  
2  
3  
4  
5  
6  
7  
8  
9  
10  
11  
12  
13  
14  
15  
16  
17  
18  
19  
20  
21  
22  
23  
24  
25  
26  
27  
28  
29  
30  
31  
32  
33  
34  
35  
36  
37  
38  
39  
40  
41  
42  
43  
44  
45  
46  
47  
48  
49  
50  
51  
52  
53  
54  
55  
56  
57  
58  
59  
60

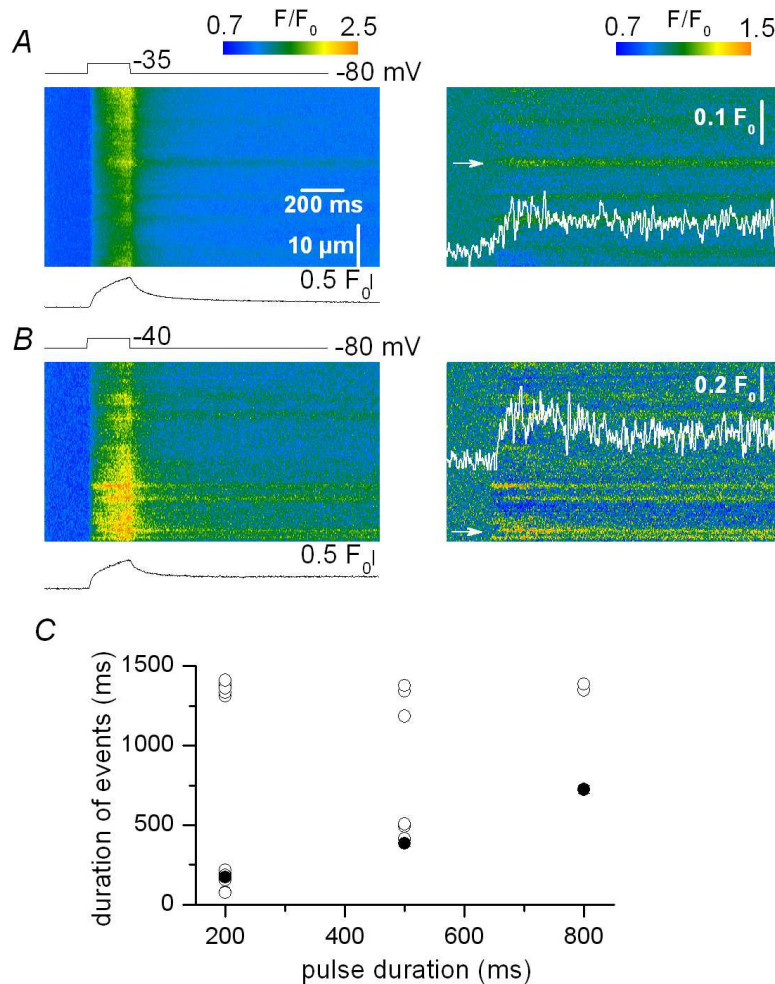
length of the pulse; data are from 13, 121 and 15 events for pulses of 200, 500 and 800 ms duration, respectively. Error bars correspond to the standard deviation.

197x288mm (150 x 150 DPI)

For Peer Review



Reconstruction of the SR  $\text{Ca}^{2+}$  release flux. A, B, cumulative distribution of latencies ( $cD(\text{lat})$ ) and of time to channel closure ( $cD(\text{ttcc})$ ) from  $\text{Ca}^{2+}$  release events elicited by 500 ms long depolarizations. C, time course of SR permeability calculated as  $cD(\text{lat}) \cdot (1 - cD(\text{ttcc}))$ . D,  $\text{Ca}^{2+}$  release flux (open squares) estimated from the global calcium transient obtained from averaging the  $F/F_0$  images in the spatial domain (thin line). Global  $\text{Ca}^{2+}$  release was calculated using a removal model (see Szentesi et al., 2004).  
286x201mm (150 x 150 DPI)

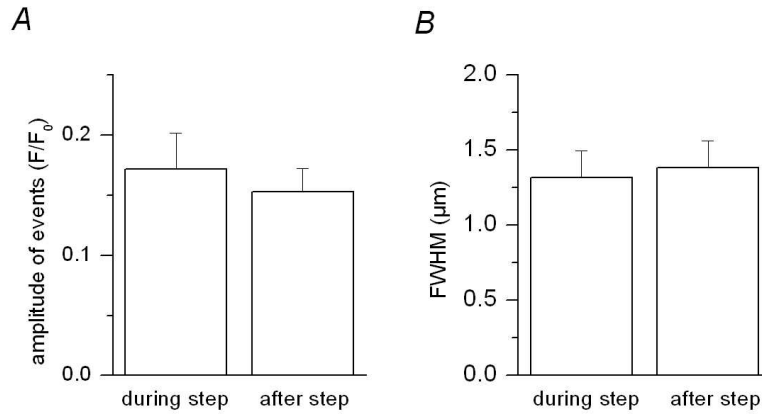


Voltage-activated  $\text{Ca}^{2+}$  release events in the presence of Maurocalcine. A-B, baseline corrected ( $F/F_0$ ) line-scan images of fluo-3 fluorescence (left) and corresponding filtered images (right, see Methods) from two distinct mouse skeletal muscle fibers depolarized by 200 ms long voltage-clamp pulses to -35 mV and -40 mV, respectively. The two fibers were injected with a solution containing 0.5 mM maurocalcine (see Methods). C, dependence of the values for the duration of the events in maurocalcine-injected fibers (open circles) versus the length of the pulse; filled circles correspond to the mean values in control fibers (see text for details).

197x288mm (150 x 150 DPI)

For Peer Review

1  
2  
3  
4  
5  
6  
7  
8  
9  
10  
11  
12  
13  
14  
15  
16  
17  
18  
19  
20  
21  
22  
23  
24  
25  
26  
27  
28  
29  
30  
31  
32  
33  
34  
35  
36  
37  
38  
39  
40  
41  
42  
43  
44  
45  
46  
47  
48  
49  
50  
51  
52  
53  
54  
55  
56  
57  
58  
59  
60



Amplitude and duration of the Ca<sup>2+</sup> release events non-interrupted by membrane repolarization in the presence of Maurocalcine. A, B, mean values for the amplitude and FWHM of the events during and after the end of the depolarization (n=11).  
201x286mm (150 x 150 DPI)